RESEARCH PAPER

Architectures of YF$_3$:Eu^{3+} solid and hollow sub-microspheres: a facile arginine-assisted hydrothermal synthesis and luminescence properties

Guixia Liu · Xia Li · Xiangting Dong · Jinxian Wang

Abstract Solid and hollow YF$_3$:Eu^{3+} spheres assembled by nanorods have been successfully synthesized via a facile arginine-assisted hydrothermal method and followed by a subsequent heat-treatment process. The experimental results reveal that the as-prepared YF$_3$:Eu^{3+} spheres are composed of the nanorods with a diameter of 20–50 nm and a length of 200–500 nm, the morphologies of YF$_3$:Eu^{3+} have been changed from solid to hollow spheres assembled by nanorods. With increase of hydrothermal temperature and time, the diameter of YF$_3$:Eu^{3+} spheres can be controlled from 300 to 800 nm. The solid and hollow spheres show an intense orange red emission peak near 595 nm, corresponding to the $^5D_0 \rightarrow {^7F_1}$ transition of Eu^{3+}. The possible formation mechanism for the hollow spheres has been presented in detail. This amine acid-assisted method is very simple, economic and environmental friendly for organic-free solvent, which would be potentially used in synthesizing other hollow materials.

Keywords YF$_3$:Eu^{3+} · Hollow spheres · Arginine · Luminescence materials · Nanocomposite

G. Liu (✉) · X. Li · X. Dong · J. Wang
School of Chemistry and Environmental Engineering,
Changchun University of Science and Technology,
Changchun 130022, China
e-mail: liuguixia22@yahoo.com.cn

Introduction

Recently, the nano- or micro- structural materials with precise architectural manipulation remain a research focus, in which hollow structures have attracted more and more interest due to their low effective densities, large surface area, interesting optical properties (Yang et al. 2008). They have a lot of potential applications in areas such as catalysis, chromatography, protection of biologically active agents, fillers, waste removal, and large bimolecular-release system (Jiang et al. 2001; Ikeda et al. 2006; Wei et al.2008; Lou and Archer 2008; Zhu et al. 2005; Yan et al. 2009). Many methods have been used to prepare hollow nano- or micro-spheres, such as template-directed synthesis with hard templates (Caruso et al.1998; Jia et al. 2009, 2010) or soft templates (Putlitz et al. 2001; Zhang et al. 2010; Zhang et al. 2002; Peng et al. 2003), microemulsion or reverse microemulsion methods, self- organization, and self-interface reactions (Wang et al. 1993; Huang et al. 2000; Bao et al. 2003; Li et al. 2004).

Amino acid has special functional groups (–NH$_2$ and –COOH) and some electron donor elements (O, N and S), it can be capable of linking with metal ions (Stumm et al. 1981, 1970; Sillen and Martell 1964; Sillen and Martell 1971). Thus amino acid can be used as templates for directing the self-assembly of the materials. More and more researchers have focused on using amino acids as surfactants to prepare architectural nanomaterials with various

morphologies. For instance, 3D and 1D structures of CdS with controlled size and shape were synthesized in the presence of cysteine (Xiong and Xi 2007). Flowerlike bismuth sulfide assembled by nanorods were prepared with the aid of cysteine by hydrothermal method (Zhang et al. 2006a). The same as in the presence of cysteine, antimony sulfide nanowires were prepared (Chen et al. 2005).The trigonal tellurium nanowires with sharp end were obtained in the presence of L-lysine (Mayers and Xia 2002). CeO_2 dumbbell-shaped, bundles and hemisphere were synthesized using L-lysine, L-glutamic and L-aspartic, separately (Zhang et al. 2006b).

Rare earth fluoride nanomaterials have potential application in optics, optoelectronics, microelectronics, and tribology, due to their low non-radiation transitions, good optical properties and lower phonon energy (Wang and Li 2003). Many methods have been applied to synthesize RE-doped fluoride luminescence nanomaterials. For example, CeF_3 hollow nanostructures with different morphologies have been prepared by hydrothermal approach (Wu et al. 2008). $LaF_3:Eu^{3+}$ nanoparticles were prepared by refluxing method in glycerol/water mixture (Wang et al. 2009). $YF_3:Eu^{3+}$ with different crystalline phases and morphologies were synthesized via a facile hydrothermal route (Zhong et al. 2009). Uniform $YF_3:Eu^{3+}$ disk-like superstructures were prepared via a solvothermal method (Wang et al. 2008c) Optical properties of RE-doped YF_3 crystalline nano-materials have been investigated extensively(Cao et al. 2008; Wang et al. 2008a; Tao et al. 2007). However, to the best of our knowledge, it is rarely reported that amino acid-assisted method to synthesize RE-doped fluoride luminescence nanomaterials, and this kind of hollow $YF_3:Eu^{3+}$ sphere assembled by nanorods has not been reported.

Herein, we report a facile and environmental friendly arginine-assisted hydrothermal method to prepare $YF_3:Eu^{3+}$ solid and hollow spheres constructed from nanorods, and the formation mechanism and photoluminescence properties are discussed.

Experimental section

In this work, the primary chemicals used were yttrium oxide(Y_2O_3, 99.99%), europium oxide(Eu_2O_3, 99.99%) purchased from Shanghai Yuelong Non-Ferrous Metals

Limited, China, L-arginine(L-$C_6H_{14}N_4O_2$, 99.99%, Shanghai Huishi Biochemical Reagents Limited, China), ammonium fluoride (NH_4F, A.R., Tianjin Kermel Chemical Reagents Limited, China) and HNO_3(A.R., Beijing Chemical Company, China). All chemicals used directly without any further purification.
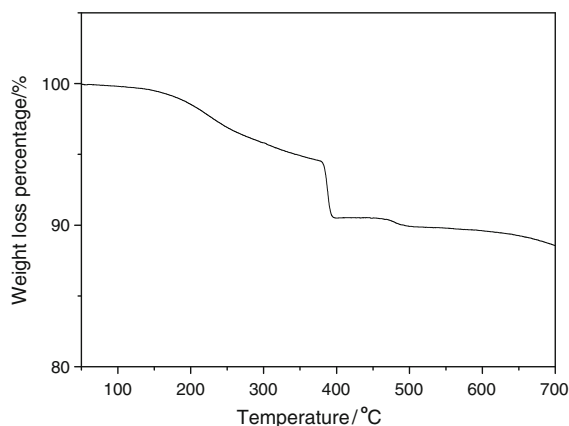
In a typical experiment, first, rare-earth oxides (Y_2O_3, Eu_2O_3) were dissolved by heating in diluted HNO_3 ($V_{H_2O}:V_{HNO_3} = 1:1$) to prepare 0.1 mol L^{-1} $Y(NO_3)_3$ and 0.05 mol L^{-1} $Eu(NO_3)_3$ solution, respectively. Secondly, 24 mL $Y(NO_3)_3$ and 2.5 mL $Eu(NO_3)_3$ was mixed together to form rare earth nitrate solutions according to the molar ratio of Y:Eu = 95:5, then 9 mL L-arginine solution was added dropwise by stirring for 0.5 h to form a clear transparent solution, in which the molar ratio of rare earth ion and L-arginine is 1:3. Then 1.5 mol L^{-1} NH_4F solution (the molar ratio of rare earth ions to NH_4F is 1:3) was introduced dropwise to the above stirred solution. After additional agitation for 0.5 h, the resulting solution was transferred into a 50 mL Teflon-lined autoclave, sealed and heated at 120, 160, 200 °C for 1, 6, 12, 24 and 48 h, respectively. The autoclave was cooled to room temperature naturally. The precursors were separated by centrifugation and washed three times with double-distilled water and ethanol, dried at 50 °C for 6 h. The final white products were obtained through a heat treatment at 450 °C in air for 4 h with a heating rate of 1 °C·min^{-1}.

The phase structures of the products were identified by power X-ray diffraction (XRD) using a Rigaku D/max-RA X-ray diffractometer with CuKa$_1$ radiation ($\lambda = 1.5406$ Å). The size and morphology of the products were observed using field emission scanning electron microscopy (FESEM; XL-30, FEI) and transmission electron microscopy (TEM; JEM-2010, JEOL). Fourier Transform Infrared Spectrometer (FT-IR) absorption spectra were performed with a Shimadzu Corporation 8400S infrared spectrophotometer with the KBr pellet technique. Thermogravimetric analysis (TGA) data were recorded with a thermal analysis instrument (SDT-2960, PERKIN-ELMER) with a heating rate of 10 °C min^{-1} in flowing air. The photoluminescence properties of the products were characterized with a HITACHI F-4500 Fluorescence Spectrophotometer equipped with a 150 W Xenon lamp as the excitation source at room temperature, the slit is 2.5 nm, the scanning ranges from 200 to 800 nm, the step is 0.2 nm and the scanning rate is 1200 nm min^{-1}.

Results and discussion

Thermogravimetric analysis (TGA) curve of as-prepared precursors before calcination is shown in Fig. 1. From the curve, we can see that there are three stages of weight loss. The first stage (weight loss: 0.47%) observed between 100 and 180 °C is attributed to the presence of absorbed surface water. The second stage (weight loss: 8.8%) ranges from 180 to 390 °C, corresponding to the decomposition of complex formed by arginine and rare earth ions. The third stage (weight loss: 2.2%) ranged from 390 to 450 °C is assigned to the removal of organic remains. There is no further change in weight above 450 °C. Therefore, the calcination temperature of the $YF_3:Eu^{3+}$ precursors in our experiments is set to 450 °C. In order to remove impurity adequately, the time of thermal treat is extended to 4 h.

Figure 2 shows the XRD patterns of the precursors for hydrothermal reaction at 120, 160 and 200 °C, respectively. It is noted that the XRD patterns all appear strong and sharp peaks, indicating that the precursor samples are well-crystallized, but they could not be indexed to the available literature values. It is deduced that the unknown diffraction patterns may be the complex formed by the groups of arginine and rare earth ions (Burford et al. 2003). The XRD patterns of the calcined samples are shown in Fig. 3, we can see that after calcined at 450 °C for 4 h, the data of all the diffraction peaks are in good agreement with the literature values (JCPDS Card No. 74-0911), which suggests that the pure orthogonal phase YF_3 is successfully obtained, the lattice

constant is $a = 6.353$ Å, $b = 6.850$ Å, $c = 4.393$ Å. The result coincides with the TG analysis. At the same time, the crystal structure of YF_3 has not been changed after doping with Eu^{3+} ion. In addition, the diffraction intensities of the samples for hydrothermal reaction at 200 °C are stronger than that of the other two samples, revealing that the crystal grows well.

In order to give further information about the composition of the samples, FT-IR spectra were characterized, as shown in Fig. 4. In Fig. 4a, it is observed that the strong peaks near 1700–1561 cm^{-1} are assigned to the vibration of $-NH_2$ and the C=O stretching vibration of $-COOH$ group ($\nu_{C=O}$) (Wang
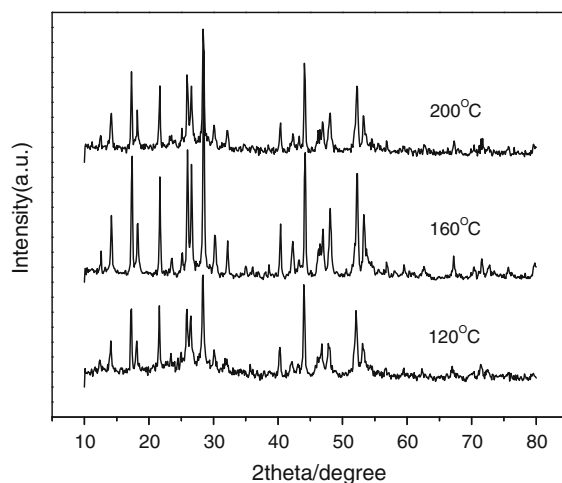
Fig. 2 XRD patterns of the precursors prepared at different hydrothermal reaction temperatures

Fig. 1 TG curve of the precursors
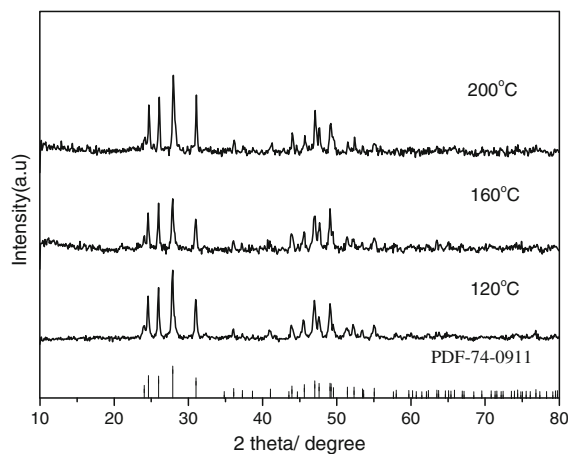
Fig. 3 PDF card(74-0911)and XRD patterns of the calcined samples at different hydrothermal temperatures
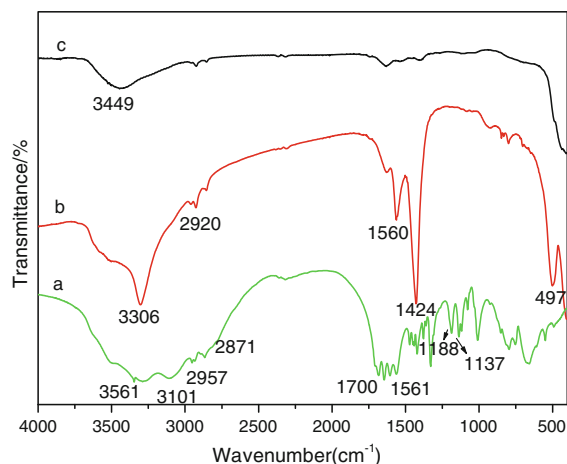
Fig. 4 FTIR patterns of pure L-C$_6$H$_{15}$N$_4$O$_2$ (*a*); as-prepared precursors (*b*) and the samples calcinated at 450 °C (*c*) for hydrothermal reaction at 200 °C

et al. 2008c), the strong and broad bands near 3561–3101 cm^{-1} are the stretching vibration of O–H in –COOH group ($v_{O–H}$), the peaks near 2957 and 2871 cm^{-1} are ascribed to the asymmetric (v_{as}) and symmetric (v_s) stretching vibration of methylene (–CH$_2$) in the arginine molecule, respectively, the peaks near 1188 and 1137 cm^{-1} are due to the vibration of amine (–C–N), these peaks are the characteristic absorption peaks of L-arginine. Compared with Fig. 4a, we can see the differences in the as-prepared precursors (Fig. 4b), some characteristic absorption peaks of L-arginine disappear, and the new peaks near 1560 and 1424 cm^{-1} are ascribed to the asymmetric (v_{as}) and symmetric (v_s) stretching vibration of the carboxylic group (–COO$^-$), respectively, which indicates that the complex has been formed. An adsorption peak near 497 cm^{-1} in the fingerprint region is attributed to Y–O stretching band in the complex. After calcinating at 450 °C for 4 h in the air (Fig. 4c), it can be seen that no obvious absorption peaks. It is thought that most residual organic molecules are combusted at high temperature, and YF$_3$:Eu^{3+} is formed by calcined at 450 °C. The result coincides with the XRD results.
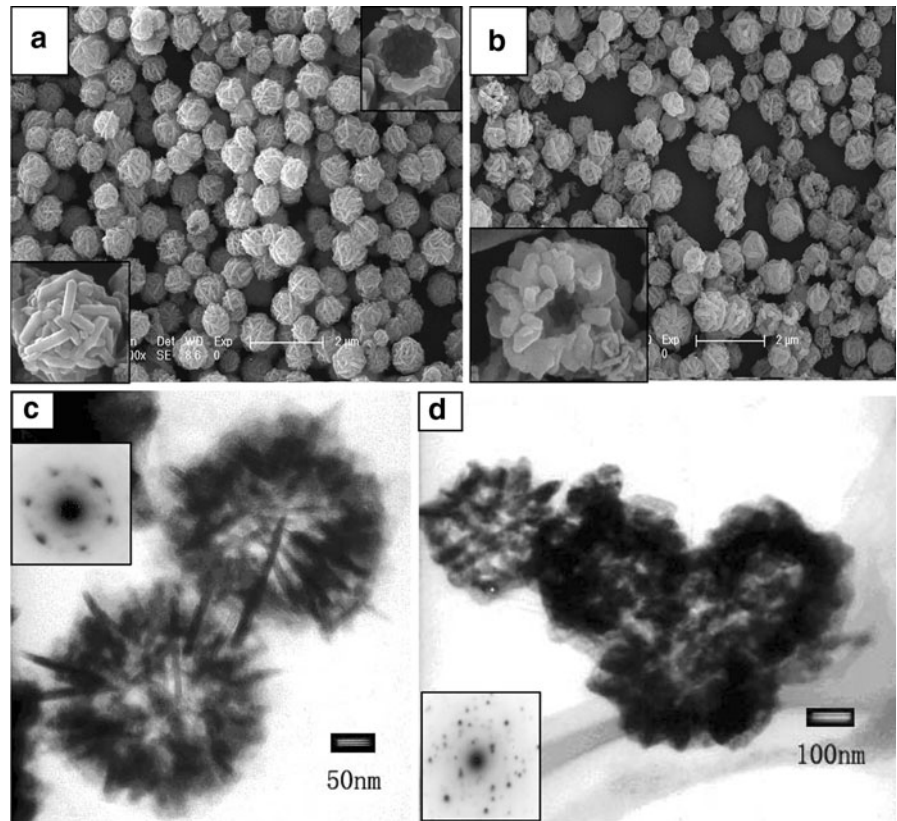
The morphologies of the as-prepared precursors and the samples calcined at 450 °C for reaction at 200 °C for 24 h are observed by FESEM and TEM, the images are shown in Fig. 5. From Fig. 5a and b, it is noted that the precursors and the calcined samples are all in hollow spheres with a diameter of 500–800 nm. In addition, it can be clearly seen from the high magnification images

that the hollow spheres are composed of some regular nanorods with an average diameter of 20–40 nm and a length from 200 to 500 nm. TEM images (Fig. 5c, d) further confirm the central hollow shapes of the precursors and YF$_3$:Eu^{3+} samples, which agrees well with the FESEM observations. The SEAD patterns (inset in Fig. 5c, d) of the precursors and the YF$_3$:Eu^{3+} samples show diffuse rings and dots, confirming that the samples are polycrystalline.

In order to further understand the formation of YF$_3$:Eu^{3+} hollow structure, time-dependent experiments were carried out while keeping the other reaction conditions unchanged. Figure 6 shows the FESEM images of the YF$_3$:Eu^{3+} samples for different hydrothermal reaction times (1, 6, 12 and 48 h). It is noted that when the reaction time is 1 h (Fig. 6a), the samples are all in sphere shapes with a diameter of 300–500 nm and well monodispersed distribution, the spheres are assembled by nanorods. When the hydrothermal reaction time reaches 6 h (Fig. 6b), the morphologies have not changed and the sizes increase little, the average diameter of the sphere-like structure is 500–800 nm, and the spheres are assembled by the nanorods with an average diameter of 50 nm and a length of 200–500 nm. Increasing the reaction time to 12 h (Fig. 6c), the sizes also increase little. When increasing the reaction time to 24 h, see from Fig. 5, a clear hollow interior appears in the center of the spheres. And when prolonging the reaction time to 48 h (Fig. 6d), the spheres are still hollow. On the basis of above analysis, the influence of reaction time on hollow structure is important but on the size of the spheres is few. The formation of the YF$_3$:Eu^{3+} hollow sphere is believed to be the result of the Ostwald ripening process, which instructs the growth and re-crystallization with enough ripening time. During the process, the inner crystallites would dissolve and disappear, and produce the hollow structure.

Hydrothermal temperature has also played a crucial role in the formation of the hollow spheres assembled by nanorods. The morphologies of the calcined samples for hydrothermal reaction at 120 and 160 °C were further characterized by FESEM and TEM, as shown in Fig. 7. When the Hydrothermal temperature is 120 °C, uniform and monodispersed spheres with an average diameter of about 800 nm were obtained. It can be seen that the samples are all solid spheres assembled by nanorods and the surfaces are not very smooth (Fig. 7a, c). The TEM

Fig. 5 FESEM images of as-prepared precursors (**a**) and samples calcined at 450 °C (**b**) (the inset is high magnification images); TEM images of as-prepared precursors (**c**) and samples calcined at 450 °C (**d**) (the insets are SEAD photos) for hydrothermal temperature at 200 °C for 24 h

Fig. 6 FESEM images of samples calcined at 450 °C at different hydrothermal reaction time (**a** 1 h, **b** 6 h, **c** 12 h, **d** 48 h)(the inset is high magnification images)
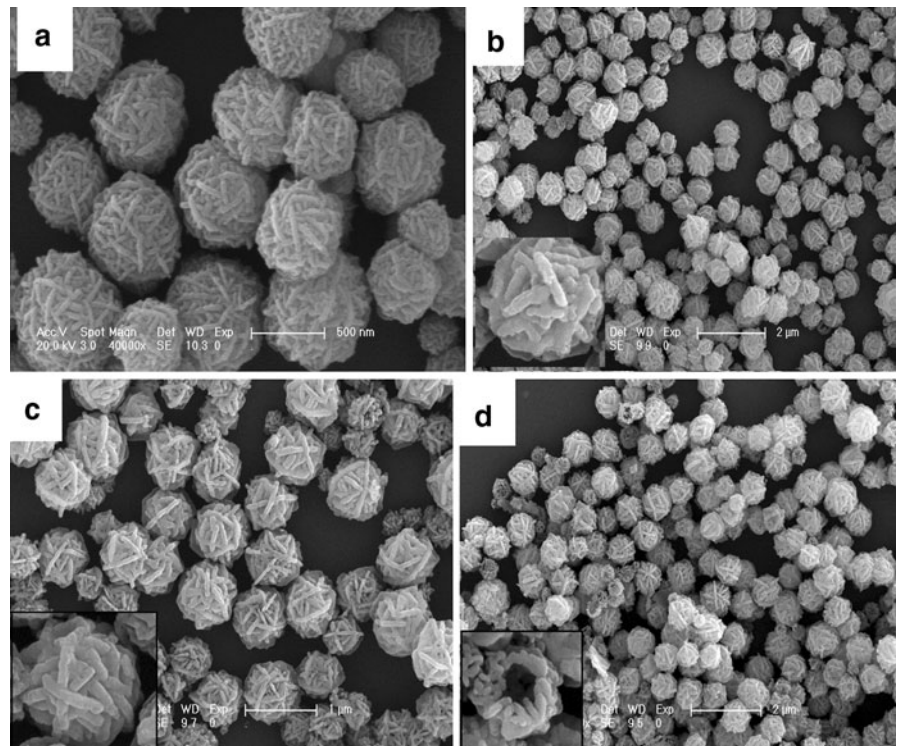
Fig. 7 FESEM images of the as-prepared precursors (**a**, **b**) and the calcined samples (**c**, **d**) (**a**, **c** for hydrothermal temperature at 120 °C and **b**, **d** for hydrothermal temperature at 160 °C), TEM images of calcined samples for hydrothermal temperature at 120 °C (**e**) and for hydrothermal temperature at 160 °C (**f**)
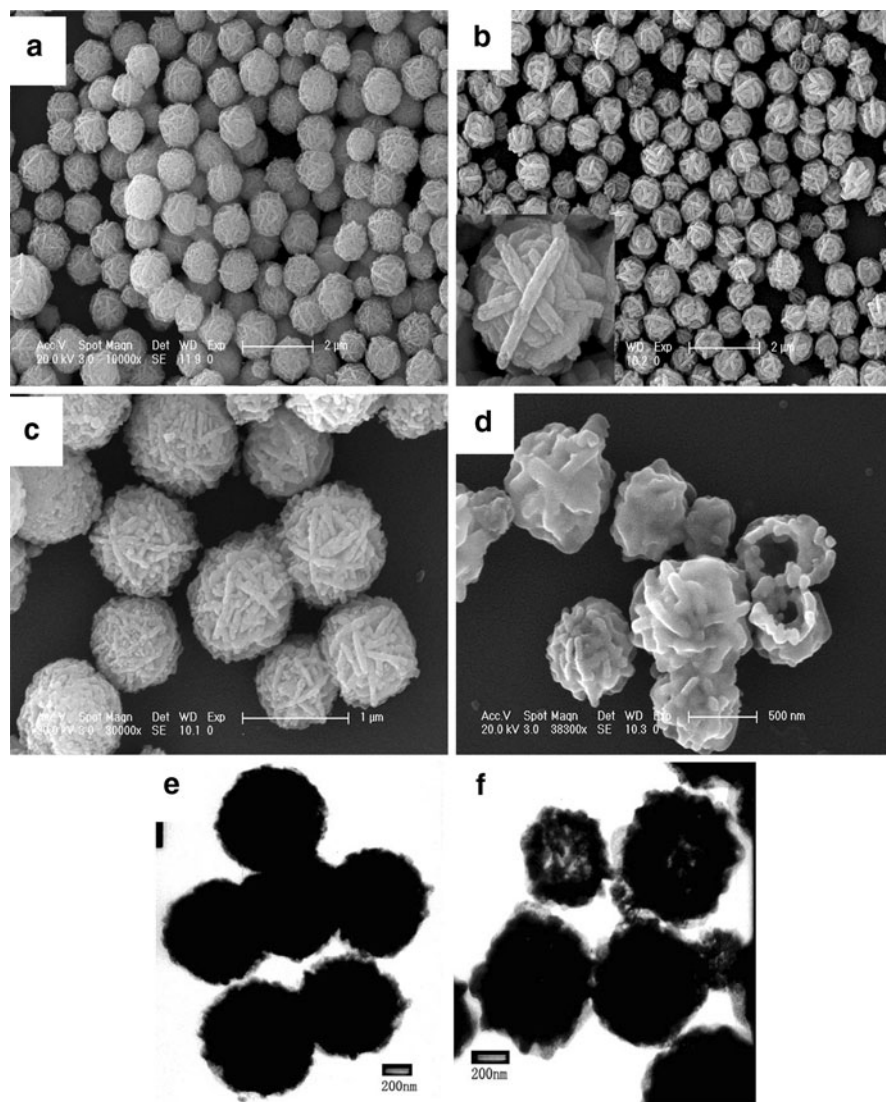

image (Fig. 7e) further indicated that the spheres are solid. With the temperature rising to 160 °C, partial spheres appear hollow structure composed of nanorods (Fig. 7b, d, f). With a further increase in the hydrothermal reaction temperature, namely at 200 °C, the hollow spheres are obtained (Fig. 5). We can conclude that the hydrothermal temperature and reaction time have key effects on the formation of the obtained hollow spheres.

In this paper, L-arginine here is used as an assembly agent, it plays a key role in the formation of YF₃:Eu³⁺ spheres and self-assembly of the nanorods, and the hydrothermal temperatures and times are also important for the formation of YF₃:Eu³⁺ hollow spheres. The possible formation mechanism of YF₃:Eu³⁺

hollow sphere is investigated as shown in Fig. 8. In the beginning of the process, it is supposed that L-arginine may combine with Y(Eu)³⁺ to form complex under hydrothermal conditions (From XRD results). The similar result had been reported (Burford et al. 2003), they put forward that the metal ions could react with L-cysteine to form stable complex. With the adding of the NH₄F, the complex reacts with F⁻, by the guidance of the linear structure of L-arginine, 1D nanorods are formed and self-assembled to sphere structures. Under the given hydrothermal temperature and time, that is more than 160 °C and 24 h, the Ostwald ripening process would instruct the inner crystallites to dissolve and disappear, then the solid spheres transfer into the hollow structure. At the same

**Fig. 8** The possible formation mechanism of YF$_3$:Eu^{3+} hollow spheres
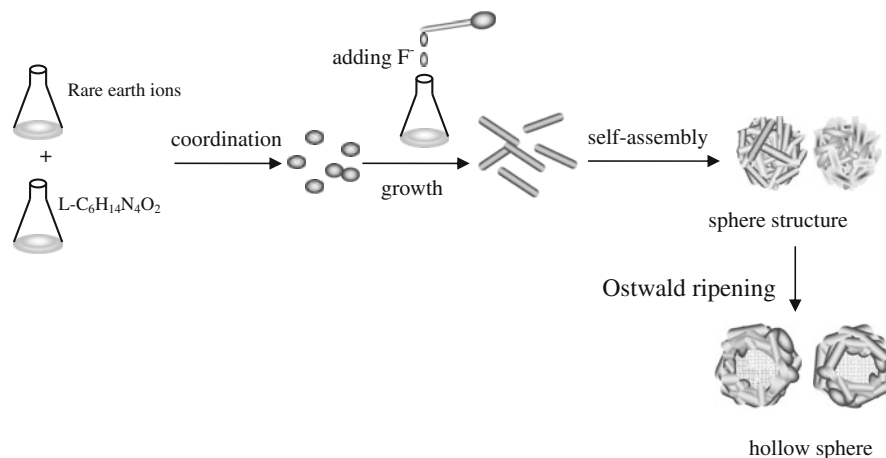
time, the released NH$_3$ gas decomposed from L-arginine would provide basic environment and act as soft template to form hollow structure.
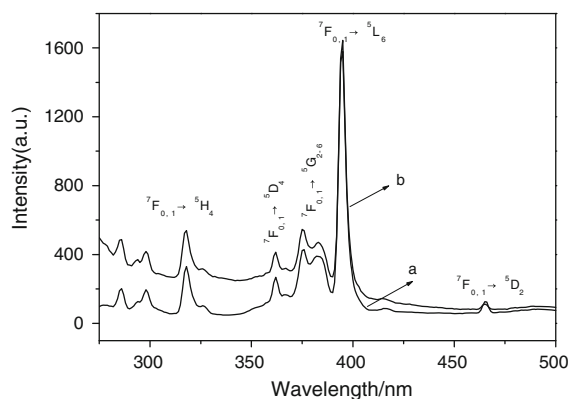
Figure 9 exhibits emission spectra of the precursors (a) and the calcined samples (b) for hydrothermal reaction at 200 °C for 24 h. The two emission spectra consist of lines located from 500 to 750 nm. These lines correspond to transitions from the excited $^5D_{0,1,2}$ levels to ^7F_J ($J = 1$–4) energy levels of 4f^6 configuration in Eu^{3+}. The emission peaks are observed at 511, 527, 556, 589(595), 616(622), 652, 692(701) nm, which attributed to the $^5D_2 \rightarrow {}^7F_3$, $^5D_1 \rightarrow {}^7F_1$, $^5D_1 \rightarrow {}^7F_2$, $^5D_0 \rightarrow {}^7F_1$, $^5D_0 \rightarrow {}^7F_2$, $^5D_0 \rightarrow {}^7F_3$, $^5D_0 \rightarrow {}^7F_4$ transitions, respectively (Wang et al. 2008b). The most intense peaks are centered at 595(589) nm, corresponding to the magnitic-dipole transitions. And the intensity of $^5D_1 \rightarrow {}^7F_1$ transition is much stronger than that of the $^5D_0 \rightarrow {}^7F_2$

transition, indicating good monochromaticity and the inversion symmetry of the Eu^{3+} site(Tao et al. 2007). Comparing curve a with curve b, the relative luminescent intensity of the calcined samples is about three times higher than that of the precursors.

Figure 10 depicts the excitation spectra of the precursors (a) and the calcined samples (b). A series of narrow absorption lines correspond to the direct excitation of the europium ground state into higher excited states of the europium f-electron. The most intense peak is centered at 395 nm, corresponding to $^7F_0 \rightarrow {}^5L_6$ transition, which is the characteristic absorption peaks of Eu^{3+}(Yan and Li 2005). The spectra are reported for other Eu^{3+} doped materials (Lorbeer et al. 2010). Similar with the emission spectra, the excited intensity of the calcined samples is stronger than that of the precursors.
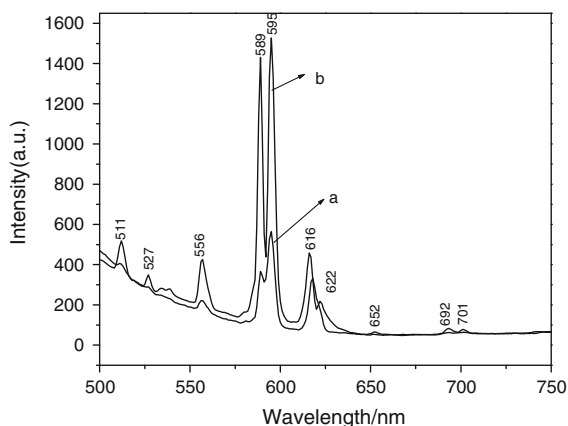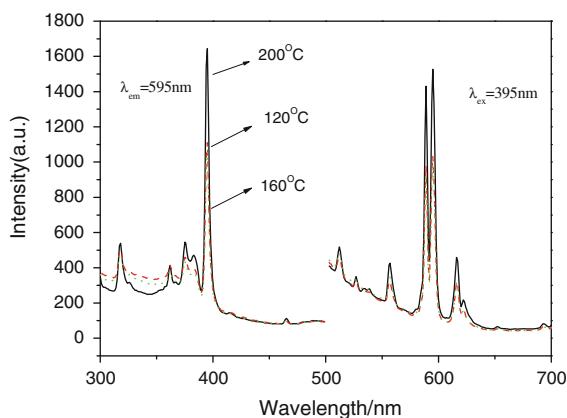

Fig. 9 Emission spectra of the precursors (**a**)and the calcined samples (**b**) for hydrothermal reaction at 200 °C ($\lambda_{ex} = 395$ nm)
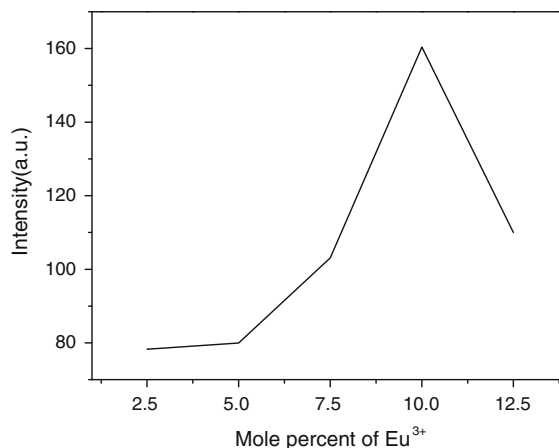

Fig. 10 Excitation spectra of the precursors (**a**) and the calcined samples (**b**) for hydrothermal reaction at 200 °C ($\lambda_{em} = 595$ nm)

Figure 11 shows the PL spectra of the $YF_3:Eu^{3+}$ samples for different hydrothermal reaction temperatures. The $YF_3:Eu^{3+}$ hollow spheres (200 °C) exhibit the strong luminescent intensity at 595 nm in emission spectra and 395 nm in the excitation spectra. Comparatively, the as-prepared solid spheres (120 °C) and the partial hollow spheres (160 °C) present the lower weak emission. In the previous report (Cong and Yu 2007), the hollow spheres had weaker emission than that of the solid spheres because of their larger surface area. But in our experiments, the $YF_3:Eu^{3+}$ hollow spheres show stronger luminescent intensity than that of the solid sphere and partial hollow sphere. Combining with the XRD patterns, the diffraction intensity of the samples (200 °C) is the strongest, which indicated that the excellent crystallinity has a key role in the luminescent intensity. The results suggest that the luminescent intensity not only depends on the surface area and low densities, but also the crystallinity of the samples.

Figure 12 illustrates the relationship between the luminescence intensity ($^5D_0 \rightarrow {}^7F_1$) and the doping concentration of Eu^{3+} ions for the calcined samples for hydrothermal reaction at 200 °C. The Eu^{3+} concentration was varied from 2.5 mol% to 12.5 mol%. It can be seen that the emission intensity gradually increases with the increase of Eu^{3+} concentration, the sample with a doped concentration of 10 mol% shows the highest emission intensity. When the Eu^{3+} doping concentration exceeds to 10 mol%, the emission intensity decreases. The phenomenon of concentration quenching occurs. So the quenching concentration of the hollow $YF_3:Eu^{3+}$ is about

Fig. 12 Dependence of luminescence intensity of the $^5D_0 \rightarrow {}^7F_1$ transition on Eu^{3+} doping concentration of the calcined samples for hydrothermal reaction at 200 °C

10 mol%. The quenching concentration is mainly determined by the structure characteristic of the host and the particle size(Li et al.2007).

Conclusions

In summary, the hollow sphere-like structure of $YF_3:Eu^{3+}$ composed of nanorods has been successfully synthesized by a facile arginine-assisted hydrothermal method. The hydrothermal temperature and reaction time have played crucial role in controlling the spheres from solid to hollow spheres. The as-prepared spheres have characteristic orange red emission of Eu^{3+}, the calcined samples have a higher PL intensity than that of the precursors, and the quenching concentration of $YF_3:Eu^{3+}$ hollow spheres is about 10 mol%. This amine acid-assisted method has great potential to prepare other hollow materials for its facile and economic.

Fig. 11 Excitation spectra (left) and Emission spectra (right) of the calcined samples for different hydrothermal temperatures

References

Bao JC, Liang YY, Xu Z, Si L (2003) Facile synthesis of hollow nickel submicrometer spheres. Adv Mater 15:1832–1835. doi:10.1002/adma.200305315

Burford N, Eelman MD, Mahony DE, Morash M (2003) Definitive identification of cysteine and glutathione complexes of bismuth by mass spectrometry: assessing the biochemical fate of bismuth pharmaceutical agents. Chem Commun 146–147. doi:10.1039/b210570e

Cao CY, Qin WP, Zhang JS (2008) Enhanced ultraviolet up-conversion emissions of Tm^{3+}/Yb^{3+} codoped YF_3 nanocrystals. J Fluor Chem 129:204–209. doi:10.1016/j.jfluchem.2007.11.002->

Caruso F, Caruso RA, Mohwald H (1998) Nanoengineering of inorganic and hybrid hollow spheres by colloidal templating. Science 282:1111–1114

Chen XY, Zhang XF, Shi CW, Li XL, Qian YT (2005) A simple biomolecule-assisted hydrothermal approach to antimony sulfide nanowires. Solid State Commun 134:613–615. doi:10.1016/j.ssc.2005.03.004

Cong HP, Yu SH (2007) Hybrid ZnO-dye hollow spheres with new optical properties by a self-assembly process based on evans blue dye and cetyltrimethylammonium bromide. Adv Funct Mater 17:1814–1820. doi:10.1002/adfm.200601082

Huang JX, Xie Y, Li B, Liu Y, Qian YT, Zhang SY (2000) In situ Source–Template–Interface reaction route to semiconductor CdS submicrometer hollow spheres. Adv Mater 12:808–811. doi:10.1002/(SICI)1521-4095(200006)

Ikeda S, Ishino S, Harada T, Okamoto N, Sakata T, Mori H, Kuwabata S, Torimoto T, Matsumura M (2006) Ligand-free platinum nanoparticles encapsulated in a hollow porous carbon shell as a highly active heterogeneous hydrogenation catalyst. Angew Chem Int Ed 45:7063–7066. doi:10.1002/anie.200602700

Jia G, Yang M, Song YH, You HP, Zhang HJ (2009) General and facile method to prepare uniform Y_2O_3:Eu hollow microspheres. Cryst Growth Des 9(1):301–307

Jia G, You HP, Liu K, Zheng YH, Guo N, Zhang HJ (2010) Highly uniform Gd_2O_3 hollow microspheres: template-directed synthesis and luminescence properties. Langmuir 26(7):5122–5128

Jiang P, Bertone JF, Colvin VL (2001) A lost-wax approach to monodisperse colloids and their crystals. Science 291:453–457

Li XL, Lou TJ, Sun XM, Li YD (2004) Highly sensitive WO_3 hollow-sphere gas sensors. Inorg Chem 43:5442–5449. doi:10.1021/ic049522w

Li YC, Chang YH, Lin YF, Chang YS, Lin YJ (2007) Synthesis and luminescent properties of Ln^{3+} (Eu^{3+}, Sm^{3+}, Dy^{3+})-doped lanthanum aluminum germanate $LaAlGe_2O_7$ phosphors. J Alloys Compd 439(1–2):367–375. doi:10.1016/j.jallcom.2006.08.269

Lorbeer C, Cybinska J, Mudring AV (2010) Facile preparation of quantum cutting GdF_3:Eu^{3+} nanoparticles from ionic liquids. Chem Commun 46:571–572. doi:10.1039/b919732j

Lou XW, Archer LA (2008) A general route for non-spherical anatase TiO_2 hollow colloids and magnetic multifunctinal particls. Adv Mater 20:1853–1858

Mayers B, Xia YN (2002) One-dimensional nanostructures of trigonal tellurium with various morphologies can be synthesized using a solution-phase approach. J Mater Chem 12:1875–1881. doi:10.1039/B201058E

Peng Q, Dong Y, Li Y (2003) ZnSe semiconductor hollow microspheres. Angew Chem Int Ed 42:3027–3030

Putlitz BZ, Landfester K, Fischer H, Antonietti M (2001) The generation of "armored latexes" and hollow inorganic shells made of clay sheets by templating cationic mini-emulsions and latexes. Adv Mater 13:500–503. doi:10.1002/1521-4095(200104)

Sillen LG, Martell AE (1964) Stability constants of metal-ion complexes. Chem Soc London Spec Publ 17

Sillen LG, Martell AE (1971) Stability constants of metal-ion complexes. Chem Soc London Spec Publ 25

Stumm W, Morgan JJ (1981) Aquatic Chemistry. An introduction emphasizing chemical equilibriain natural waters, seconded. Wiley-Interscience, NY

Stumm W, Huang P, Jenkins R (1970) Specific chemical interactions affecting the stability of dispersed systems. Croat Chem Acta 42:223–244

Tao F, Wang ZJ, Yao LZ (2007) Synthesis and photoluminescence properties of truncated octahedral Eu-doped YF_3 submicrocrystals or nanocrystals. J Phys Chem C 111(8):3241–3245. doi:10.1021/jp065905z

Wang X, Li Y (2003) Fullerene-like rare-earth nanoparticles. Angew Chem Int Ed 42:3497–3500

Wang W, Fu XA, Tang JA, Jiang L (1993) Preparation of submicron spherical particles of silica by the water-in-oil microemulsion method. Colloids Surf A 81:177–180. doi:10.1016/0927-7757(93)80244-9

Wang GF, Qin WP, Zhang JS (2008a) Enhancement of violet and ultraviolet upconversion emissions in Yb^{3+}/Er^{3+}-codoped YF_3 nanocrystals. Opt Mater 31:296–299. doi:10.1016/j.optmat.2008.04.013

Wang GF, Qin WP, Zhang JS (2008b) Synthesis and spectral properties of Eu^{3+}-doped YF_3 nanobundles. J Fluor Chem 129:621–624. doi:10.1016/j.jfluchem.2008.05.003

Wang SJ, Xu HL, Chen XS (2008c) Solvothermal synthesis of disk-like YF_3 superstructures. J Cryst Growth 310:4697–4700. doi:10.1016/j.jcrysgro.2008.09.003

Wang ZL, Lin J, Li M (2009) Photoluminescence properties of LaF_3:Eu^{3+} nanoparticles prepared by refluxing method. J Rare Earths 27(1):33–37. doi:10.1016/S1002-0721(08)60185-4

Wei W, Ma GH, Hu G, Yu D, Mcleish T, Su ZG, Shen ZY (2008) Preparation of hierarchical hollow $CaCO_3$ particles and the application as anticancer drug carrier. J Am Chem Soc 130:15808–15810. doi:10.1021/ja8039585

Wu Q, Chen Y, Xiao P, Zhang F, Wang XZ, Hu Z (2008) Hydrothermal synthesis of cerium fluoride hollow nanostructures in a controlled growth microenvironment. J Phys Chem C 112:9604–9609. doi:10.1021/jp800838y

Xiong SL, Xi BJ (2007) Synthesis of 3D and 1D structures of CdS in a binary solution with L-cysteine's assistance. Chem Eur J 13:3076–3081

Yan RX, Li YD (2005) Down/up conversion in Ln^{3+}-doped YF_3 nanocrystals. Adv Funct Mater 15:763–770. doi:10.1002/adfm.200305044

Yan E, Ding Y, Chen C, Li R, Hu Y, Jiang X (2009) Polymer/silica hybrid hollow nanospheres with pH-sensitive drug release in physiological and intracellular environments. Chem Commun 2718–2720

Yang J, Li CX, Quan ZW, Zhang CM, Yang PP, Li YY, Yu CC, Lin J (2008) Self-assembled 3D flowerlike Lu_2O_3 and Lu_2O_3:Ln^{3+} (Ln = Eu, Tb, Dy, Pr, Sm, Er, Ho, Tm) microarchitectures: ethylene glycol-mediated hydrothermal

synthesis and luminescent properties. J Phys Chem C 112:12777–12785. doi:10.1021/jp803945w

Zhang D, Qi L, Ma J, Cheng H (2002) Synthesis of submicrometer-sized hollow silver spheres in mixed polymer-surfactant solutions. Adv Mater 14:1499–1502

Zhang B, Ye XC, Hou WY, Zhao Y, Xie Y (2006a) Biomolecule-assisted synthesis and electrochemical hydrogen storage of Bi_2S_3 flowerlike patterns with well-aligned nanorods. J Phys Chem B 110:8978–8985. doi:10.1021/jp060769j

Zhang GJ, Shen ZR, Liu M (2006b) Synthesis and characterization of mesoporous ceria with hierarchical nanoarchitecture controlled by amino acids. J Phys Chem B 110: 25782–25790. doi:10.1021/jp0648285

Zhang LH, Jia G, You HP, Liu K, Yang M, Song YH, Zheng YH, Huang YJ, Guo N, Zhang HJ (2010) Sacrificial template method for fabrication of submicrometer-sized $YPO_4:Eu^{3+}$ hierarchical hollow spheres. Inorg Chem 49:3305–3309. doi:10.1021/ic9022739

Zhong SL, Wang SJ, Xu HL (2009) Facile synthesis of water-soluble YF_3 and $YF_3: Ln^{3+}$ nanocrystals. Mater Lett 63:530–532. doi:10.1016/j.matlet.2008.11.003

Zhu YF, Shi JL, Shen WH, Dong XP, Feng JW, Ruan ML, Li YS (2005) Novel stimuli-responsive controlled drug release from a hollow mesoporous silica sphere/polyelectrolyte multilayers core-shell structure. Angew Chem Int Ed 44:5083–5087